Journal of Inorganic Biochemistry 136 (2014) 1–12

Contents lists available at ScienceDirect

Journal of Inorganic Biochemistry

journal homepage: www.elsevier.com/locate/jinorgbio

Influence of PPh_3 moiety in the anticancer activity of new organometallic ruthenium complexes

Rubén Sáez [a], Julia Lorenzo [b], Ma Jose Prieto [c], Mercè Font-Bardia [d], Teresa Calvet [d], Nuria Omeñaca [e], Marta Vilaseca [e], Virtudes Moreno [a,*]

[a] Department de Química Inorgànica, Facultat de Química, Universitat de Barcelona, Martí y Franquès 1-11, 08028 Barcelona, Spain
[b] Institut de Biotecnologia i Biomedicina, Universitat Autònoma de Barcelona, 08193 Barcelona, Spain
[c] Departament de Microbiologia, Facultat de Biologia, Universitat de Barcelona, Diagonal 645, 08028 Barcelona, Spain
[d] Departament de Cristal·lografia, Mineralogia i Dipòsits Minerals, Universitat de Barcelona, Martí i Franquès s/n., 08028 Barcelona, Spain
[e] IRB Barcelona-Institute for Research in Biomedicine, Parc Científic de Barcelona, Baldiri Reixac, 10-12, 08028 Barcelona, Spain

ARTICLE INFO

Article history:
Received 21 July 2013
Received in revised form 3 March 2014
Accepted 6 March 2014
Available online 15 March 2014

Keywords:
Arene ruthenium(II) complexes
Ruthenium antitumor compounds
pBR322 DNA
Calf thymus DNA
DNA interaction
Protein interaction

ABSTRACT

The effect of the PPh_3 group in the antitumor activity of some new organometallic ruthenium(II) complexes has been investigated. Several complexes of the type $[Ru^{(II)}(Cl)(PPh_3)(Lig\text{-}N)]$, $[Ru^{(II)}(Cl)_2(Lig\text{-}N)]$ (where Lig-N = pyridine derivate) and $[Ru^{(II)}(Cl)(PPh_3)_2]$, have been synthesized and characterized. A noticeable increment of the antitumor activity and cytotoxicity of the complexes due to the presence of PPh_3 moiety has also been demonstrated, affording IC_{50} values of 5.2 μM in HL-60 tumor cell lines. Atomic force microscopy, circular dichroism and electrophoresis experiments have proved that these complexes can bind DNA resulting in a distortion of both secondary and tertiary structures. Ethidium bromide displacement fluorescence spectroscopy studies and viscosity measurements support that the presence of PPh_3 group induces intercalation interactions with DNA. Indeed, crystallographic analysis, suggest that intra-molecular π–π interactions could be involved in the intercalation within DNA base pairs. Furthermore, high performance liquid chromatography mass spectrometry (HPLC–MS) studies have confirmed a strong interaction between ruthenium complexes and proteins (ubiquitin and potato carboxypeptidase inhibitor — PCI) including slower kinetics due to the presence of PPh_3 moiety, which could have an important role in detoxification mechanism and others. Finally, ion mobility mass spectrometry (IMMS) experiments have proved that there is no significant change in the gas phase structural conformation of the proteins owing to their bonding to ruthenium complexes.

1. Introduction

In the last few years, ruthenium complexes have attracted much attention as building blocks for new transition-metal-based antitumor agents, since they present some advantages over platinum complexes currently used in cancer chemotherapy [1,2]. Ruthenium compounds show less toxicity, a novel mechanism of action, the prospect of non-cross-resistance [3,4] and a different spectrum of activity [5,6]. More concretely, organometallic ruthenium(II) complexes with arene ligands represent an important group of ruthenium compounds with anticancer activity that is being intensively studied in the last decades [7]. The typical structure of organometallic ruthenium complexes bearing η^6-arene ligands is shown in Fig. 1, which consist in a half-sandwich "piano-stool" $[(\eta^6\text{-arene})Ru(X)(Y)(Z)]$ complex, where X is usually a monodentate leaving group and Y, Z can be monodentate or chelating ligands, depending on the porpoise of the design [8,9].

These half sandwich "piano-stool" type constructs offer much scope for design, with the potential for modifications to the arene and its substituents (R), the monodentate leaving group (X), the ligands Y and Z, and overall charge of the complex (n+). These features provide handles for the control of both the thermodynamics and kinetics of these systems as well as their overall structural architecture, allowing a more rational drug design approach compared to platinum-based drugs [10]. They also provide an ability to fine-tune the chemical reactivity of the complexes, potentially allowing the control of pharmacological properties including cell uptake, distribution, and interactions with biomolecules, toxic side effects, and detoxification mechanisms [11].

With regard to their mechanism of action, the role of the arene moiety, as well as the influence of the other ligands on the aqueous chemistry of several complexes have been widely investigated [12–18], resulting in a complex structure–activity relationship [7]. As observed for other ruthenium complexes, their cytotoxicity is usually correlated with DNA binding [19–21], although recent works point to other biomolecules as possible biological targets. As an example, RAPTA complexes do not show selective binding to DNA in vitro, and proteins and RNA appear to be the main intracellular targets [22]. In

* Corresponding author.
E-mail address: virtudes.moreno@qi.ub.es (V. Moreno).

http://dx.doi.org/10.1016/j.jinorgbio.2014.03.002
0162-0134/

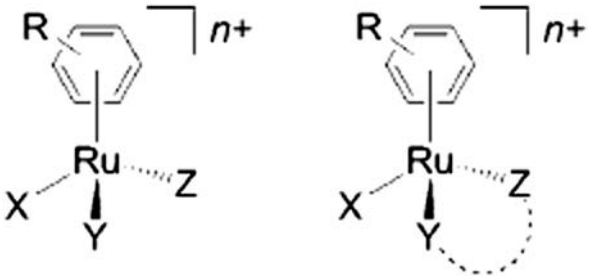

Fig. 1. Organometallic ruthenium(II) complex structure.

the same way, in the case of the NAMI-A antimetastatic agent, it is apparent that DNA is not the target, and more likely, activity is a consequence of drug–protein interaction. This is especially interesting since the antimetastatic behavior is not unique to NAMI-A, but applicable to other classes of ruthenium complexes [23,24]. Related to these results, here we explore the interaction of η^6-arene ruthenium(II) complexes with some specific proteins.

Lastly, previous works suggests that the addition of the hydrophobic PPh_3 ligand in RAPTA complexes results in more cytotoxic and less selective drugs, presumably because of increased drug uptake [22].

With the aim of developing more potent anticancer drugs, we have synthesized and characterized six new organometallic arene–ruthenium(II) complexes, some of them including PPh_3 group in its structure. In this work we study the influence of tri-phenyl-phosphine moiety in the antitumor activity of several η^6-arene ruthenium(II) complexes, and try to elucidate the possible reason behind this phenomenon.

2. Experimental

2.1. Materials

2.1.1. Reactives

$RuCl_3$, pyridine derivated ligands and methyl-benzylamines, were purchased from Fluka. KPF_6, NH_4PF_6, salts used for buffer preparation, mobile phases and ubiquitin were commercial products from Sigma-Aldrich. Solvents were purchased from Sigma-Aldrich and Panreac. Ligand *dppz* was synthesized from Sigma-Aldrich commercial products. PCI was extracted directly from potato.

2.1.2. Solutions and buffers

TE: 10 nM tris-HCl (tris-[hydroxymethyl]aminomethane hydrochloride), 0,1 mM EDTA (ethylenediaminetetraacetic acid), 50 mM NaCl; pH was adjusted to 7.4 with NaOH.

TBE: 45 mM tris-base (tris-[hydroxymethyl]aminomethane), 45 mM boric acid, 1 mM EDTA (ethylenediaminetetraacetic acid); pH was adjusted to 8 with NaOH.

HEPES: 40 mM de HEPES (4-(2-hydroxyethyl)-1-piperazineethane sulfonic acid), 10 mM $MgCl_2$; pH was adjusted to 7.4 with NaOH.

Color marker: bromophenol blue (0.25%), xilencianol FF (0.25%), glycerol 25%.

PBS: 150 mM NaCl, 3 mM KCl, 9 mM Na_2PO_4, 1.3 mM K_2PO_4; pH was adjusted to 7.2 with NaOH.

2.1.3. DNA and general materials for DNA experiments

DNA calf thymus highly polymerized sodium salt (SIGMA); Plasmid pBR322 0.25 μg/μl (Boehringer Mannheim GmbH); Agarose AG-200 molecular biology grade (ECOGEN); ethidium bromide (MERCK).

2.1.4. Protein solutions preparation. Proteins: Ubiquitin and potato carboxypeptidase inhibitor (PCI)

Ubiquitin 3 mM solution was prepared dissolving commercial lyophilized ubiquitin in mQ water. PCI solution 1.86 mM was prepared dissolving the protein directly extracted from potato, in mQ water. Protein concentration was determined in both cases through absorbance measurements with UV–visible (UV–Vis) spectrophotometer CARY 100 SCAN (Varian) as predicted by Lambert–Beer theory. Molar absorptivity coefficient estimation was made with the method proposed by Grimsley et al. [25].

2.2. Devices and methods

2.2.1. X-ray diffraction analysis

Crystal structures were registered with an ENRAF-NONIUS CAD4. Software for structure refining was SHELXS97 and SHELXL97. Crystals were obtained through diethyl ether slow diffusion in saturated dichloromethane solutions of the compounds.

2.2.2. Elemental analysis

Elemental analysis of (C, H, N, S) was carried out with a CARLO ERBA EA1108.

2.2.3. Infrared spectroscopy

IR spectra between 4000 and 600 cm^{-1} were registered with a spectrophotometer NICOLET 5700 FT-IR, in solid phase in KBr matrix.

2.2.4. NMR spectroscopy

^1H, $^{31}P\{^1H\}$ and $^{19}F\{^1H\}$ NMR were registered in a 300 MHz VARIAN UNITY. Samples were dissolved in $CDCl_3$.

2.2.5. Atomic force microscopy (AFM)

Atomic force microscopy images were obtained in TMAFM mode with a NANOSCOPE III MULTIMODE AFM from Digital Instruments Inc.

Sample preparation: DNA was treated for 15 min at room temperature to obtain a homogeneous topoisomer distribution. Stock solution 1 mg/ml was prepared in a maximum rate DMSO:HEPES 6:4, for non water soluble complexes. It was then diluted 1:1000 in HEPES until a final volume of 2000 μl, and therefore filtered through FP030/3 0.2 nm pore filters (Schleicher & Schuell GmbH). Each sample consists of 1 μl of pBR-322 plasmid DNA (0.25 μg/μl), 2 μl of drug filtered solution and then carried to a final volume of 50 μl with HEPES. Samples were incubated during 5 and 24 h at 37 °C. 2 μl of each sample are adsorbed over a mica disk (Ashville-Schoonmaker Mica Co., Newport News), washed with mQ water and dried under argon or nitrogen.

2.2.6. Circular dichroism

Circular dichroism spectra were registered with a spectropolarimeter JASCO 810, equipped with a 450 W Xenon arc lamp.

Sample preparation: 1 mg/ml stock solutions of each compound were prepared immediately before using in a DMSO:TE sterilized mixture (2% DMSO maximum). 20 μg/ml calf thymus DNA solution was prepared in TE and stored at 4 °C. DNA quantization was verified by UV–Vis spectroscopy, checking absorbance at 260 nm in a split double beam SHIMADZU UV-2101-PC spectrophotometer. Compound-DNA adduct formation was carried out by addition of solution stock aliquots of each compound to a fixed volume of DNA solution. Amount of drug added in each case is expressed as r_i (theoretical molar ratio compound–nucleotide) and is calculated as can be seen in the additional information.

$$r_i = \frac{m \times Mnucl \times Am}{C \times Mr \times V}$$

m	mass of compound used to prepare stock solution (μg)
M_{nucl}	average molecular mass by nucleotide (g/mol)
Am	number of metallic atoms in compound
C	DNA solution concentration (μg/ml)

Mr molecular mass of each compound (g/mol)
V sample final volume (ml)

All experiments were carried out for molar ratios of 0.1, 0.3 and 0.5, which means that in each case there are 1, 3 and 5 molecules of compound respectively versus each ten pairs of DNA nitrogen bases. Through this formula the μg of compound (or μl of stock solution) that must be added to DNA solution in each case can be calculated. The sample holder had 5 l/min nitrogen flow purge. 1 cm path length quartz cells were used for measurements. Each sample was registered twice in a wavelength interval of 220 and 330 nm, rate of 50 nm/min.

2.2.7. Agarose gel electrophoresis

Electrophoresis experiments were carried out in an ECOGEN horizontal tank connected to a PHARMACIA GPS 200/400 variable tension source. Gel images were recorded with a thermal system FUJIFILM FTI-500.

Sample preparation: stock solution preparation for each compound was the same to the one described for circular dichroism. Buffer solution was TE (2% DMSO maximum). Sample final volume was 20 μl:2.8 μl of DNA pBR322 solution 0.25 μg/μl, the volume of stock solution necessary to obtain the desired molar ratio ($r_i = 0.5$), and filling until 20 μl with TE buffer solution. In this way, the final concentration of DNA plasmid was 35 μg/ml so each sample contained 0.7 μg of DNA. After incubation at 37 °C for 24 h of 20 μl compound-DNA solution samples 4 μl of color marker was added. The mixture went through electrophoresis in 0.5% agarose gel in TBE buffer at 1.5 V/cm for 4 h. After that DNA was stained with ethidium bromide solution (0.5 μg/ml in TBE) during 20 min. Negative control was a free plasmid pBR322 DNA solution, and for positive control cisplatin–DNA samples in the same conditions of all other complexes were prepared.

2.2.8. Molecular fluorescence

Fluorescence molecular emission measurements were registered with a spectrofluorimeter Kontron SFM-25 (*Bio-Tek Instruments*).

Sample preparation: several 3 ml aliquots from a calf thymus DNA 50 μM standard stocking solution were taken, adding to them necessary amount (30 μl) of ethidium bromide 5 mM to get 1:1 molar ratio, and they were incubated for 30 min at 37 °C. Afterwards, growing amounts (0, 20, 40, 60, 80 y 100 μl) of compound stock solution (1.5 mM DMSO/mQ water) were added to different samples, to obtain different complex concentrations in each one (0, 10, 20, 30, 40 y 50 μM respectively). Emission spectra were registered between 530 and 670 nm and excitation wavelength was established in 502 nm. DMSO concentration in final samples was always below 2%.

2.2.9. Viscosity measurements

DNA solutions viscosity measurements were carried out with a Vibro Viscometer SV-1[a] (*AND A&N Company Limited*).

Sample preparation: 1 ml stock solution 5 mM of each compound in DMSO/water (4:1), and 1 mM calf thymus DNA solution were prepared. Afterwards, several aliquots of 1 ml from this last were transferred to different sterilized tubes, adding then 3 ml of TE buffer, which corresponds with DNA control solution. For each compound, increasing amounts of stock solution (20, 60 and 100 μl) were added to reach molar ratios of 0.1, 0.3 and 0.5 DNA: complex, respectively. In all of them viscosity at 25 °C was measured before and after mixing, and along the time as well (0, 4, 14, 32, 44 and 56 h), keeping constant temperature with a termostatized water bath for the samples and isobuthyl alcohol bath for viscometer devices. Again, DMSO concentration in biological samples did not exceed 2%.

2.2.10. Mass spectrometry

Matrix-assisted laser desorption ionization-time of flight (MALDI-TOF) mass spectra were obtained with a VOYAGER DE-RP (Applied Biosystems) mass spectrometer provided with a nitrogen laser (337 nm, 3 ns pulsed) and applying 20–25 KV as accelerating voltages. Samples were dissolved in suitable matrixes (DHB 2,5-dihydroxybenzoic acid, Sigma-Aldrich, 10 mg/ml acetonitrile/H_2O 1:1 volume (0.1% TFA)).

Infusion high resolution electrospray ionization mass spectrometry (ESI-MS) spectra were carried out with a LC/MSD-TOF (*Agilent Technologies*) mass spectrometer provided with double nebulizer for exact mass determination. (See Table S1 in Supplementary information for experimental condition details).

Liquid chromatography mass spectrometry (LC–MS) experiments were performed on a QSTAR Elite System Hybrid Quadrupole-TOF LC/MS/MS (AB Sciex) using an Agilent 1100 G13112B pump, and an Agilent 1200 G1367C automatic sampler provided with a column oven.

Potato carboxypeptidase inhibitor (PCI)-complex and ubiquitin-complex adducts (where complex = 1.7), were obtained by aqueous solution reaction at neutral pH and temperature of HPLC autosampler (40 °C). Aliquots of 300 μl of PCI and ubiquitin solutions were taken, and it was added with the necessary amount (μl) of 0.01 M compound stock solution (DMSO/mQ water, 2% maximum DMSO) to obtain 1:1 molar ratio. The system was allowed to react and its evolution was studied by HPLC–MS with 10 μl sample injection per hour, during 24 h. A Nucleosil 120 C18 10 μm 25 × 0.45 cm column was used for chromatographic separation using linear gradients of acetonitrile in aqueous solution (A: ammonium acetate 0.01 M, B: acetonitrile 0–100% flux: 1 ml/min–40 min). A 1:10 split post-column was done for on-line coupling to the mass spectrometer. Experimental mass spectrometry conditions are described in the Supplementary information (Table S2).

2.2.11. Ion mobility mass spectrometry (IMS–MS)

IMS–MS experiments were carried out using a SYNAPT G1 HDMS mass spectrometer (Waters, Manchester, UK). Samples were placed on a 384-well plate refrigerated at 15 °C and introduced by automated chip-base nanoelectrospray using a Triversa NanoMate (Advion Bio-Sciences) in positive ion mode. A reduction of the source pumping speed in the backing region (5.81 mbar) of the mass spectrometer was done for optimal ion transmission. (For detailed experimental conditions see Supplementary Table S3) The instrument was calibrated over the m/z range 500–5000 Da using a solution of cesium iodide. MassLynx vs 4.1 SCN 704 software and Driftscope vs 2.1 software were used for data processing. Experimental drift times were transformed into collision cross sections (CCS, Ω) by constructing a calibration curve with proteins of known collision cross-sections. The calibrant lists are given in Table S4 and the calibration curves are shown in Fig. S2. Experimental drift times for these calibrants were recorded using identical instrument conditions than the studied complexes.

They were taken 10 μl of 3 mM ubiquitin solution and 20 μl of 1.86 mM PCI solution, and it was added with the necessary volume of complex E1 and E2 0.01 M stock solutions to obtain 1:1 molar ratio. Samples were incubated for 24 h at 37 °C. Afterwards they were diluted with 600 μl of ammonium acetate buffer, and 10 μl of this diluted solution was poured in the sample plate of the Advion Triversa Nanomate. DMSO concentration never exceeded 2%.

2.2.12. In vitro cytotoxicity and apoptosis assays on HL-60 cells

2.2.12.1. Tumor cell lines and culture conditions. The cell line used was the human acute promyelocytic leukemia cell line HL-60 (American Type Culture Collection (ATCC)). Cells were routinely maintained in RPMI-1640 medium supplemented with 10% (v/v) heat inactivated fetal bovine serum, 2 mmol/l glutamine, 100 U/ml penicillin, and 100 lg/ml streptomycin (Gibco BRL, Invitrogen Corporation, Netherlands) in a highly humidified atmosphere of 95% air with 5% CO_2 at 37 C.

2.2.12.2. Cytotoxicity assays. Growth inhibitory effect of the ruthenium complexes on the leukemia HL-60 cell line was measured by the microculture tetrazolium, [3-(4,5-dimethylthiazol-2-yl)-2,5-diphenyltetrazolium bromide, MTT] assay [26]. Briefly, cells growing in the logarithmic phase were seeded in 96-well plates (104 cells per well), and then were treated with varying doses of the ruthenium complex and the reference drug cisplatin at 37 C for 24 h. For each of the variants tested, four wells were used. Aliquots of 20 μl of MTT solution were then added to each well. After 3 h, the color formed was quantified by a spectrophotometric plate reader at 490 nm wavelength. The percentage of cell viability was calculated by dividing the average absorbance of the cells treated with the complex by that of the control; IC50 values (drug concentration at which 50% of the cells are viable relative to the control) were obtained by GraphPad Prism software, version 4.0.

2.3. Synthesis

2.3.1. Synthesis of complexes without PPh_3 moiety (see Fig. S1)

2.3.1.1. Synthesis of $[Ru^{II}Cl_2(p\text{-cymene})]_2$ (1). A suspension of $RuCl_3$ (0.1 g, 0.36 mmol) in ethanol (40 ml) was heated under reflux during 8 h with 6 equivalents (2 ml, 18 mmol) of R-α-phellandrene, keeping the stirring afterwards during 12 h more at room temperature. Solvent was removed under reduced pressure until an orange precipitate was observed, which was filtered off, washed with cold methanol and dried under reduced pressure.

Yield: 65%; M.S.[ESI]: m/z 576.9 $\{M\text{-}Cl\}^+$; Anal. Calc. $C_{20}H_{28}Cl_4Ru_2$: 39.23% C, 4.61% H; Anal. Exp.: 39.39% C, 4.51% H; ^{1}H NMR [$CDCl_3$]: δ_a 5.48, δ_b 5.35 (*dd*, J(HH) ≈ 6.0 Hz, 4H, C2,3,5,6-H{ring}), δ 2.93 (*sep*, J(HH) ≈ 7.0 Hz, H, $CH(Me)_2$), δ 2.16 (*s*, 3H, CH_3{ring}), δ 1.28 (*d*, JHH ≈ 7.0 Hz, 6H, $CH(Me)_2$); IR: 3052.68 (νCsp^2–H), 2961.22 (νCsp^3–H), 1468–1386 (νC═C).

2.3.1.2. Synthesis of $[Ru^{II}Cl_2(p\text{-cymene})(4\text{-}(2\text{-EtOH})Py)]$ (2). A suspension of (1) (0.1 g, 0.16 mmol) and 4-(2-hydroxyethyl)pyridine (300 μl, 2.7 mmol) in methanol (30 ml) was heated under reflux during 7 h, keeping the stirring afterwards during 12 h more at room temperature. Solvent was removed under reduced pressure until an orange oil was obtained. With the addition of diethyl ether an orange precipitate was obtained, which was filtered off, washed with diethyl ether and dried under reduced pressure.

Yield: 83%; M.S.[ESI]: m/z 394.05 $\{M^+\text{-}Cl\}$; Anal. Calc. $C_{17}H_{22}Cl_2NORu$: 47.56% C, 5.40% H, 3.26% N; Anal. Exp.: 47.57 %C, 5.35% H, 3.35% N; ^{1}H NMR [$CDCl_3$]: δ 8.88 (*d*, J(HH) ≈ 6.2 Hz, 2H, C–H{4-(2-EtOH)Py}), δ 7.18 (*d*, J(HH) ≈ 6.2 Hz, 2H, C–H{4-(2-EtOH)Py}), δ 5.44–5.21 (*2d*, J(HH) ≈ 6.0 Hz, 4H, C–H{ring}), δ 3.80 (*m*, J(HH) ≈ 6.0 Hz, 2H, CH_2{4-(2-EtOH)Py}), δ 3.00 (*sep*, J(HH) ≈ 7.0 Hz, H, $CH(Me)_2$), δ 2.85 (*t*, J(HH) ≈ 6.0 Hz, 2H, CH_2{4-(2-EtOH)Py}), δ 2.11 (*s*, 3H, CH_3{ring}), δ 1.31 (*d*, J(HH) ≈ 7.0 Hz, 6H, $CH(Me)_2$); IR: 3463.70 (νOH), 816.35 (νRu–N).

2.3.2. Synthesis of complexes including PPh_3 moiety (see Fig. S1)

2.3.2.1. Synthesis of $[Ru^{II}Cl_2(p\text{-cymene})PPh_3]$ (3). A suspension of (1) (0.55 g, 0.9 mmol) and PPh_3 (0.6 g, 2.25 mmol) in hexane (30 ml) was heated under reflux during 5 h, keeping the stirring until it reached room temperature. The red precipitate result was filtered off, washed with hexane and dried under reduced pressure.

Yield: 82%; M.S.[ESI]: m/z 586.1 $\{M\text{-}Cl\}^+$; Anal. Calc. $C_{28}H_{29}Cl_2Ru$: 59.16% C, 5.14% H; Anal. Exp.: 58.83% C, 5.04% H; ^{1}H NMR [$CDCl_3$]: δ 7.37–7.83 (*m*, 15H, PPh_3), δ_a 5.18, δ_b 4.99 (*2d*, J(HH) ≈ 6.0 Hz, 4H, C–H{ring}), δ 2.85 (*sep*, J(HH) ≈ 7.0 Hz, H, $CH(Me)_2$), δ 1.87 (*s*, 3H, CH_3{ring}), δ 1.11 (*d*, J(HH) ≈ 7.0 Hz, 6H, $CH(Me)_2$); $^{31}P\{^1H\}$NMR [$CDCl_3$]: δ 24.16 (*s*, PPh_3); IR: 1091.21 (νP–C), 520.95 (πC–P–C).

2.3.2.2. Synthesis of $[Ru^{II}Cl(p\text{-cymene})(3\text{-picoline})PPh_3][PF_6]$ (4). A suspension of (3) (0.1 g, 0.18 mmol), KPF_6 (0.04 g, 0.2 mmol) and 3-methylpyridine (3-picoline, 400 μl, 4.0 mmol) in methanol (30 ml) was stirred during 24 h at room temperature. Solvent was removed under reduced pressure until a yellow oil was obtained. With the addition of diethyl ether a yellow precipitate was obtained, which was filtered off, washed with diethyl ether and dried under reduced pressure.

Yield: 78%; M.S.[ESI]: m/z 626.13 $\{M^+\}$; Anal. Calc. $C_{34}H_{36}ClF_6NP_2Ru$: 52.96% C, 4.71% H, 1.82% N; Anal. Exp.: 53.13% C, 4.83, 1.82% N; ^{1}H NMR [$CDCl_3$]: δ 8.76 (*d*, J(HH) ≈ 5.0 Hz, H, C–H{3-picoline}), δ 8.53 (*s*, H, C–H{3-picoline}), δ 7.27–7.57 (*m*, 16H, PPh_3, 3-picoline), δ 7.04 (*d*, J(HH) ≈ 2.0 Hz, H, C–H{3-picoline}), δ 5.95–5.30 (*4d*, J(HH) ≈ 5.0 Hz, 4H, C–H{ring}), δ 2.18 (*sep*, J(HH) ≈ 6.4 Hz, H, $CH(Me)_2$), δ 2.12 (*s*, 3H, CH_3{3-picoline}), δ 1.65 (*s*, 3H, CH_3{ring}), δ 1.10 (*2d*, J(HH) ≈ 7.0 Hz, 6H, $CH(Me)_2$); $^{31}P\{^1H\}$NMR [$CDCl_3$]: δ 37.3 (*s*, PPh_3), δ −144.1 (*sep*, J(PF) ≈ 713 Hz, PF_6^-), $^{19}F\{^1H\}$NMR [$CDCl_3$]: δ −73 (*d*, J(FP) ≈ 713 Hz, PF_6^-); IR: 1093.02 (νP–C), 840.39 (νRu–N), 700.75 (νP–F).

2.3.2.3. Synthesis of $[Ru^{II}Cl(p\text{-cymene})(3,4\text{-lutidine})PPh_3][PF_6]$ (5). A suspension of (3) (0.1 g, 0.18 mmol), KPF_6 (0.04 g, 0.2 mmol) and 3,4-dimethylpyridine (3,4-lutidine, 200 μl, 1.8 mmol) in methanol (30 ml) was heated under reflux during 7 h, keeping the stirring afterwards during 12 h more at room temperature. Solvent was removed under reduced pressure until an orange oil was obtained. With the addition of diethyl ether an orange precipitate was obtained, which was filtered off, washed with diethyl ether and dried under reduced pressure.

Yield: 84%; M.S.[ESI]: m/z 640.15 $\{M^+\}$; Anal. Calc. $C_{35}H_{38}ClF_6NP_2Ru\text{-}H_2O$: 52.34 %C, 5.02% H, 1.74% N; Anal. Exp.: 52.39% C, 4.60% H, 1.84% N; ^{1}H NMR [$CDCl_3$]: δ 8.60 (*d*, J(HH) ≈ 5.3 Hz, H, C–H{3,5-lutidine}), δ 8.35 (*s*, H, C–H{3,5-lutidine}), δ 7.26–7.5 (*m*, 15H, PPh_3), δ 6.90 (*d*, J(HH) ≈ 5.3 Hz, H, C–H{3,5-lutidine}), δ 5.98–5.28 (*4d*, J(HH) ≈ 5.7 Hz, 4H, C–H{ring}), δ 2.21 (*sep*, J(HH) ≈ 7.0 Hz, H, $CH(Me)_2$), δ 2.15 (*s*, 3H, CH_3{3,5-lutidine}), δ 1.99 (*s*, 3H, CH_3{3,5-lutidine}), δ 1.64 (*s*, 3H, CH_3 {ring}), δ 1.11 (*2d*, J(HH) ≈ 5.0 Hz, 6H, $CH(Me)_2$); $^{31}P\{^1H\}$NMR [$CDCl_3$]: δ 37.7 (*s*, PPh_3), δ −144.1 (*sep*, J(PF) ≈ 713 Hz, PF_6^-), $^{19}F\{^1H\}$ NMR [$CDCl_3$]: δ −73 (*d*, J(FP) ≈ 713 Hz, PF_6^-); IR: 1092.35 (νP–C), 840.39 (νRu–N), 700.30 (νP–F).

2.3.2.4. Synthesis of $[Ru^{II}Cl(p\text{-cymene})(3,5\text{-lutidine})PPh_3][PF_6]$ (6). A suspension of (3) (0.1 g, 0.18 mmol), KPF_6 (0.04 g, 0.2 mmol) and 3,5-dimethylpyridine (3,5-lutidine, 200 μl, 1.8 mmol) in methanol (30 ml) was heated under reflux during 7 h, keeping the stirring afterwards during 12 h more at room temperature. Solvent was removed under reduced pressure until an orange oil was obtained. With the addition of diethyl ether an orange precipitate was obtained, which was filtered off, washed with diethyl ether and dried under reduced pressure.

Yield: 89%; M.S.[ESI]: m/z 640.15 $\{M^+\}$; Anal. Calc. $C_{35}H_{38}ClF_6NP_2\text{-}Ru\text{-}H_2O$: 52.34% C, 5.02% H, 1.74% N; Anal. Exp.: 52.61% C, 4.72% H, 1.89% N; ^{1}H NMR [$CDCl_3$]: δ 8.43 (*s*, 2H, C-H{3,5-lutidine}), δ 7.27–7.50 (*m*, 15H, PPh_3), δ 7.11 (*s*, H, C–H{3,5-lutidine}), δ 5.99–5.35 (*4d*, J(HH) ≈ 5.4 Hz, 4H, C–H{ring}), δ 2.20 (*sep*, J(HH) ≈ 7.0 Hz, H, $CH(Me)_2$), δ 2.11 (*s*, 6H, $2CH_3${3,5-lutidine}), δ 1.64 (*s*, 3H, CH_3{ring}), δ 1.11 (*2d*, J(HH) ≈ 7.5 Hz, 6H, $CH(Me)_2$); $^{31}P\{^1H\}$NMR [$CDCl_3$]: δ 38.1 (*s*, PPh_3), δ −144.1 (*sep*, J(PF) ≈ 713 Hz, PF_6^-), $^{19}F\{^1H\}$NMR [$CDCl_3$]: δ −73 (*d*, J(FP) ≈ 713 Hz, PF_6^-); IR: 1092.65 (νP–C), 836.70 (νRu–N), 700.41 (νP–F).

2.3.2.5. Synthesis of $[Ru^{II}Cl(p\text{-cymene})(4\text{-}(2\text{-EtOH}))PPh_3][PF_6]$ (7). A suspension of (3) (0.1 g, 0.18 mmol), NH_4PF_6 (0.03 g, 0.2 mmol) and 4-(2-hydroxyethyl)pyridine (300 μl, 2.7 mmol) in methanol (30 ml) was heated under reflux during 7 h, keeping the stirring afterwards during 12 h more at room temperature. Solvent was removed under reduced pressure until a yellow oil was obtained. After the addition of some drops of DMSO, a brown precipitate was obtained with the

Table 1
Summary of crystallographic data.

Unit cell dimensions	(2)	(4)	(5)	(6)	(7)
Crystal system	Monoclinic	Orthorhombic	Orthorhombic	Monoclinic	Monoclinic
Space group	$P2_1/c$	Pbca	Pbca	$P2_1/c$	Cc
a	10.595 (4) Å	18.158 (6) Å	18.494 (2) Å	10.543 (6) Å	10.202 (5) Å
b	8.411 (2) Å	18.521 (6) Å	21.875 (6) Å	18.391 (8) Å	19.636 (5) Å
c	19.960 (7) Å	21.986 (3) Å	21.875 (6) Å	19.901 (8) Å	17.481 (7) Å
α	90°	90°	90°	90°	90°
β	92.31 (2)°	90°	90°	94.62 (2)°	3.00 (2)°
γ	90°	90°	90°	90°	90°

addition of H_2O. The precipitate obtained was filtered off, washed with deionized water and dried under reduced pressure.

Yield: 69%; M.S.[ESI]: m/z 656.14 $\{M^+\}$; Anal. Calc. $C_{35}H_{38}ClF_6NOP_2$-Ru-NH_4: 48.67% C, 4.74% H, 3.66% N; Anal. Exp.: 49.16% C, 4.66%, 3.57% N; ^{1}H NMR [$CDCl_3$]: δ 8.73 (*d*, J(HH) ≈ 6.3 Hz, 2H, C–H{4-(2-EtOH)Py}), δ 7.27–7.50 (*m*, 15H, PPh_3), δ 7.02 (*d*, J(HH) ≈ 6.3 Hz, 2H, C–H{4-(2-EtOH)Py}), δ 5.93–5.25 (*4d*, J(HH) ≈ 6.0 Hz, 4H, C–H{ring}), δ 3.77 (*m*, J(HH) ≈ 7.0 Hz, 2H, CH_2-{4-(2-EtOH)Py}), δ 2.76 (*t*, J(HH) ≈ 6.0 Hz, 2H, CH_2-{4-(2-EtOH)Py}), δ 2.24 (*sep*, J(HH) ≈ 7.0 Hz, H, $CH(Me)_2$), δ 1.66 (*s*, 3H, CH_3-{ring}), δ 1.10 (*d*, J(HH) ≈ 7.0 Hz, 6H, $CH(Me)_2$); $^{31}P\{^1H\}$NMR [$CDCl_3$]: δ 37.1 (*s*, PPh_3), δ −144.1 (*sep*, J(PF) ≈ 713 Hz, PF_6^-), $^{19}F\{^1H\}$NMR [$CDCl_3$]: δ −73 (*d*, J(FP) ≈ 713 Hz, PF_6^-); IR: 3533.84 (νOH), 1093.69 (νP–C), 840.42 (νRu–N), 700.86 (νP–F).

2.3.2.6. Synthesis of [Ru^{II}Cl(p-cymene)(PPh$_3$)$_2$][PF$_6$] (8). A suspension of (3) (0.1 g, 0.18 mmol), KPF_6 (0.04 g, 0.2 mmol) and PPh_3 (0.1 g, 0.4 mmol) in methanol (30 ml) was stirred during 2 h at 35 °C. Solvent was removed at room temperature under reduced pressure until a yellow oil was obtained. With the addition of hexane a yellow precipitate was obtained, which was filtered off, washed with ethanol/hexane 1:2 and dried under reduced pressure.

Yield: 78%; M.S.[ESI]: m/z 795.16 $\{M^+\}$; Anal. Calc. $C_{46}H_{44}ClF_6P_3Ru$: 58.76% C, 4.72% H; Anal. Exp.: 58.56% C, 4.79% H; ^{1}H NMR [$CDCl_3$]: δ 7.45–7.22 (*m*, 30H, $2PPh_3$), δ 5.60–5.00 (*2d*, J(HH) ≈ 6.4 Hz, 4H, C–H{ring}), δ 2.70 (*sep*, J(HH) ≈ 7.0 Hz, H, $CH(Me)_2$), δ 1.22 (*d*, J(HH) ≈ 7.0 Hz, 6H, $CH(Me)_2$), δ 1.10 (*s*, 3H, CH_3-{ring}); $^{31}P\{^1H\}$NMR [$CDCl_3$]: δ 20.67 (*s*, PPh_3), δ −144.1 (*sep*, J(PF) ≈ 713 Hz, PF_6^-), $^{19}F\{^1H\}$NMR [$CDCl_3$]: δ −73 (*d*, J(FP) ≈ 713 Hz, PF_6^-); IR: 1089.04 (νP–C), 831.44 (νRu–N), 699.03 (νP–F), 516.46 (πC–P–C).

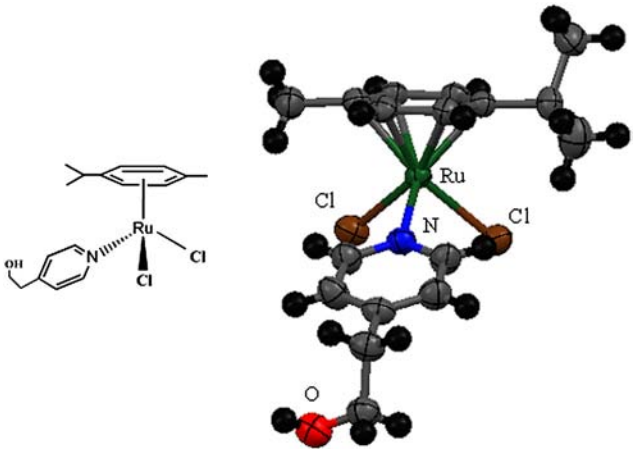

Fig. 2. ORTEP representation of crystallographic structure of complex **2**.

2.4. Crystallographic analysis

Single crystal X-ray diffraction experiments were carried out with suitable selected crystals of (**2**),(**4**),(**5**),(**6**) and (**7**), mounted at the tip of a glass fiber on an ENRAF-NONIUS CAD4 producing graphite monochromatic Mo Kα radiation (λ = 0.71073 Å). The structures were solved using the WINGX package. A summary of the crystal data can be seen in Table 1. Core length and refinements parameters are included in the Supplementary information (Tables S5). Images of each one of the complexes analyzed can be seen in Figs. 2–6. CCDC 857319–857323 contain the Supplementary crystallographic data for this paper. These data can be obtained free of charge from the Cambridge Crystallographic Data Centre via www.ccdc.cam.ac.uk/data_request/cif.

3. Results and discussions

3.1. DNA interaction studies

3.1.1. Circular dichroism

The circular dichroism spectrum of calf-thymus DNA in TE buffer shows a negative band with λ_{max} = 46 nm and a positive band with λ_{max} = 275 nm, characteristics of right-handed B-form DNA [27]. Although most of them induced changes in CD spectrum not very significant (with notable negative and positive bands intensity decrease), complex (2) and complex (8) caused important changes in ellipticity of calf thymus DNA and so distortion of its secondary structure (Fig. 7).

3.1.2. Agarose gel electrophoresis

Calf thymus DNA contains two main conformational topoisomers, open circular (OC) and covalently closed circular (CCC). Agarose gel electrophoresis studies can show the distortion of tertiary structure due to the interaction between drugs and DNA. The image in Fig. 8 shows calf thymus DNA migration through agarose gel for untreated DNA and several DNA-metallic complex adducts.

As seen below any of these complexes distorts DNA tertiary structure in a way able to change the topoisomer's distribution pattern. Only DNA–cisplatin adducts show the typical coalescence of both CC and CCC signals due to the formation of *cis* covalent bonding adducts.

These results suggest that the interaction between DNA and current ruthenium complexes could be different from the one established between DNA and cisplatin. It is well known that DNA–cisplatin adducts are preferently intrastand *cis* covalent binding, so it can be concluded that current ruthenium complexes must bind DNA in a different way, since its effect in DNA agarose gel electrophoresis migration is completely different.

3.1.3. Molecular fluorescence

Based on previous results, ethidium bromide quenching studies were carried out to elucidate whether π-stacking bonding could have any contribution to DNA ruthenium complex interaction or not. Ethidium bromide is a typical intercalator that can bond DNA nitrogen

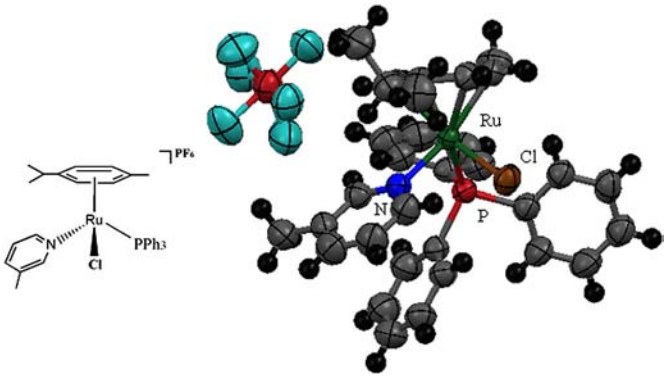

Fig. 3. ORTEP representation of crystallographic structure of complex **4**.

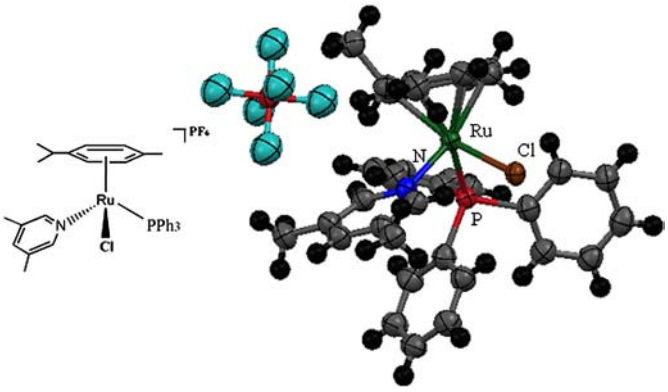

Fig. 5. ORTEP representation of crystallographic structure of complex **6**.

bases intercalating between them. Ethidium bromide displacement studies are one of the most simple and potent tools to find out if any compound can bind DNA nitrogen bases through π-stacking interaction [28].

Images on Fig. 9 show the molecular fluorescence spectra of DNA–cisplatin (negative control), DNA-9-acridine (positive control) and DNA-ruthenium complex **2** and **8** adducts. As seen below, for positive control decrease intensity of molecular fluorescence occurs when increasing drug ratio due to the consequent higher ethidium bromide displacement, and so increasing fluorescence quenching. On the other hand, negative control, shows no molecular fluorescence signal variation, as expected for compounds that are not able to stand π-stacking interactions with DNA nitrogen bases. See additional spectra for all compounds in the Supplementary information (Fig. S4).

These plots showed intensity decrease pattern for all the ruthenium complexes except for complex **2**, the only one lacking PPh_3 moiety in its structure. Different amounts of decrease was found for each one of them, achieving highest quenching values for complex **8**, since it includes two PPh_3 groups in its structure. These results suggest that PPh_3 presence could induce intercalation between nitrogen bases through π-stacking based interactions.

3.1.4. Viscosity measurements

Optical photophysical probes provide necessary, but not sufficient clues to support a binding model. Hydrodynamic measurements (i.e., viscosity and sedimentation) that are sensitive to length change are regarded as the least ambiguous and the most critical tests of a binding model in solution in absence of crystallographic structural data [29]. A classical intercalation model results in lengthening the DNA helix as base pairs are separated to accommodate the bound ligand, leading to the increase of DNA viscosity. In contrast, non-intercalative model, could bend or kink the DNA helix, reduce its effective length, and concomitantly, its viscosity. In addition, electrostatic or minor groove binding (capable of EtBr quenching in some occasions) has no influence on DNA viscosity [30]. Fig. 10 shows the change in viscosity of several calf thymus DNA solutions in TE when treated with increasing ratios of ruthenium complexes.

As seen in Fig. 10 all complexes cause an important increase in DNA solutions viscosity when increasing its concentration, except the only one lacking PPh_3 moiety in its structure. This phenomenon confirms the intercalative model induced by PPh_3 plane rings, probably in combination with pyridine derivate ring as a π-stacking sandwich system. In addition, higher increase in viscosity takes place for complex **8**, again, the one with more PPh_3 moieties included in its structure.

3.1.5. Atomic force microscopy

Ruthenium complex interaction with pBR322 DNA in HEPES buffer solution was studied by atomic force microscopy (AFM). The results obtained are depicted in Fig. 11. As can be seen, ruthenium complex binding causes DNA chain aggregation (complex **2**), DNA chain opening (complex **6**), kinks (complexes **6**, **7**), cross-linking and supercoiling (complexes **4**–**7**, remarkably complex **5**), and even chain fracture (complexes **5**, **6**), showing very different DNA morphologies related to untreated DNA.

Once more, pBR322-complex **2** system shows different topoisomer morphologies compared to the rest of ruthenium complexes, which is consistent with the intercalation binding model proposed for all of them except for complex **2**.

3.2. Protein interaction studies

Although DNA is considered as the primary target for most of the metallo-drugs studied so far [31], this belief is based mainly on studies carried out for platinum based anticancer compounds [32]. However, mechanism of action of ruthenium-based anticancer compounds is comparatively unexplored, although it is clear that ruthenium

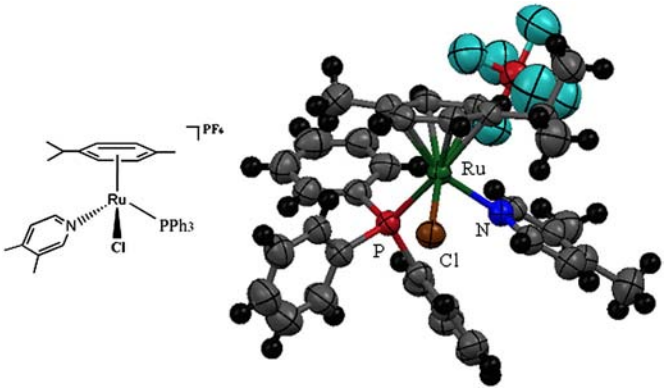

Fig. 4. ORTEP representation of crystallographic structure of complex **5**.

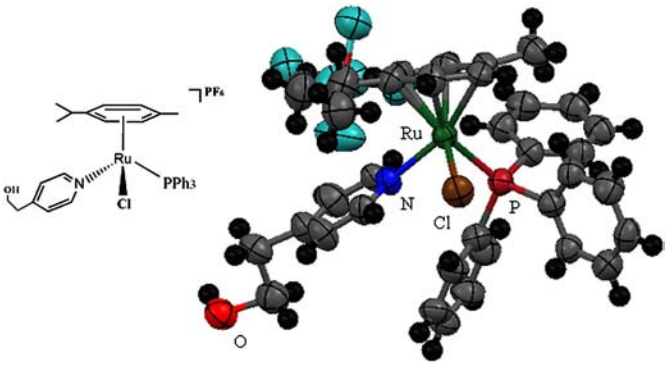

Fig. 6. ORTEP representation of crystallographic structure of complex **7**.

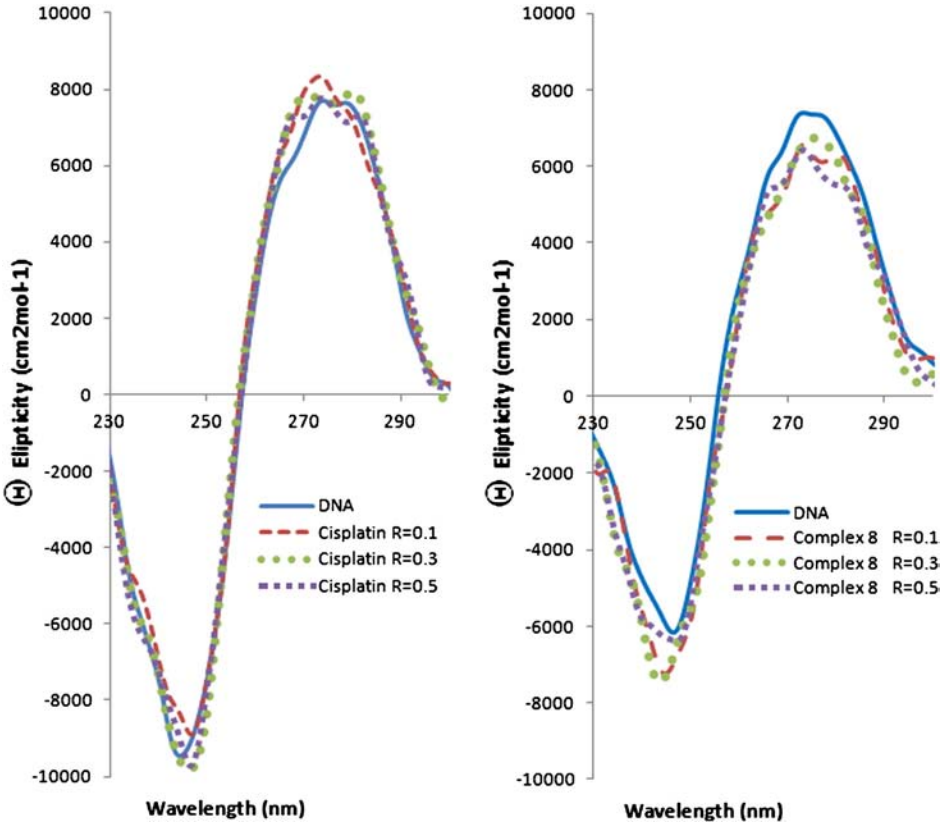

Fig. 7. CD spectra of DNA–cisplatin and DNA–complex **8** adducts.

compounds interact more weakly with DNA relative to platinum complexes [33]. There is evidence suggesting that ruthenium compounds might directly interfere with specific proteins involved in signal transduction pathways and/or alter cell adhesion and transduction processes [34–36]. With this frame, ruthenium complex reactivity studies in the presence of model and specific proteins (ubiquitin and potato carboxypeptidase inhibitor-PCI respectively) have been carried out.

Ubiquitin is a model protein that plays many different rolls in metabolism, and it is ubiquitous in the organism. On the other hand, PCI is a specific protein that can act as an antagonist of human epidermal grow factors (EGF) which are over expressed in tumor cells [37,38]. In fact, PCI is considered as a cytostatic agent, able to block the cell cycle between G_0 and G_1 phases selectively in cancer cells, without directly inducing apoptosis [39]. All these phenomena suggest the capability of PCI to vehiculize ruthenium metallo-drugs in a selective way to tumor cells (see structures of both proteins in Fig. S5 in the Supplementary information).

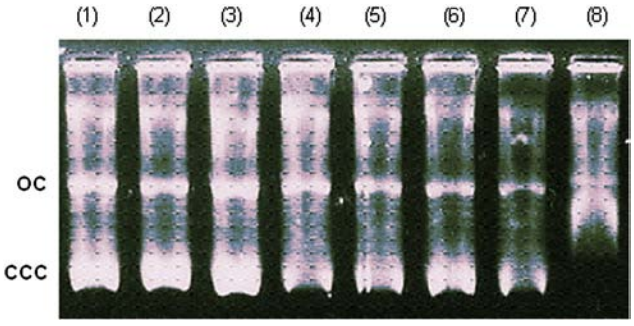

Fig. 8. Agarose gel electrophoresis image of untreated DNA (1), DNA-ruthenium complex **2**, **4**–**8** (**2**, **3**–**7**), and DNA–cisplatin (**8**) adducts.

3.2.1. HPLC–MS ruthenium complex–protein interaction study

High-resolution ESI MS has been known as a potent tool to study covalent and non-covalent ligand–biomolecule interactions [40–42] and to screen complex mixtures of metabolites, often without the need for chromatographic separation of the adducts prior to analysis [43–45]. In this case, HPLC–MS studies allowed to evaluate the interaction of ruthenium complexes with both model and specific proteins, as well as to elucidate the implications of the presence of PPh_3 moiety in this interaction.

Graphics on Figs. 12 and 13 show a summary of the decrease of free protein signal while increasing ruthenium complex–protein adduct solution content within the time (see all complete mass spectra in the Supporting information, Fig. S6).

In the case of PCI protein (Fig. 12), when PPh_3 ligand is present the kinetics of the reactions is very influenced, taking more time to detect the PCI-ruthenium complex adduct and in smaller quantities. On the other hand, when no PPh_3 moiety is present, almost all the free protein content disappears in very short period of time, to be mainly in PCI-ruthenium complex adduct form.

Added to that, for ubiquitin protein (Fig. 13), it was not possible to detect the presence of ubi-ruthenium complex adduct when PPh_3 ligand was present. All that data suggest that the PPh_3 presence affects in a very important manner to the adduct formation process kinetics, which could have very important consequences in the detoxification processes and/or in the delivery of these drugs and cell uptake, allowing slower pharmacokinetics (which usually means less secondary effects) and higher resistance to drug removal in natural detoxification processes.

3.2.2. IMMS — Ion mobility mass spectrometry studies

Ion mobility mass spectrometry can provide information on the physical size and shape of ionized molecules [46] and previous works on related Ru-based complexes have demonstrated the use of this

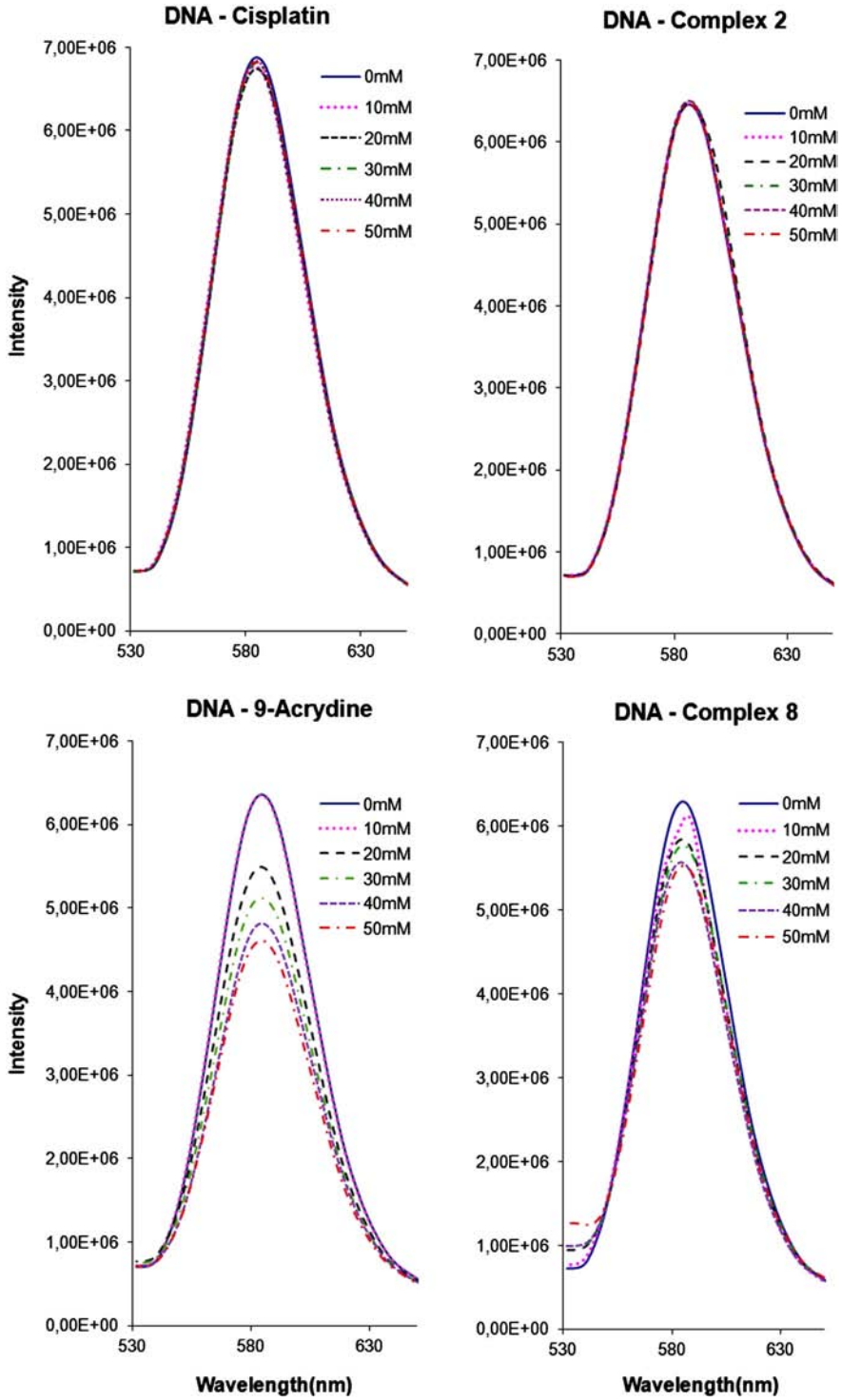

Fig. 9. Fluorescence emission spectra of DNA-EtBr system treated with some compounds showing different performances depending on the presence of PPh_3 moiety.

technique for the separation of geometrical isomers and the calculation of their collision cross-sections (CCSs) [47].

In this technique, basically, a liquid sample is ionized and injected into a drift chamber containing neutral gas at a controlled pressure (e.g., 0.5 mbar of nitrogen gas). Under the influence of an electric field, gaseous ions undergo IM separation according to the resistance they experience through their collision with neutrals, which depends on their collision cross section-to-charge ratio (Ω/z). After separation, ions are sampled by a mass spectrometer and analyzed according to their mass-to-charge (m/z) ratio. Therefore, integrated IMS–MS has the capability of separating ions not only by their mass but also by their size, shape and charge state. IM–MS offers an extra degree of analytical opportunity whereby conformational ensembles of species of equivalent mass, or the same m/z, can be separated on account of their physical shape and then mass analyzed in a single, rapid experiment. The experimental drift times (arrival times) can be correlated to collision cross sections by performing calibration curves with protein standards of known cross sections analyzed under identical

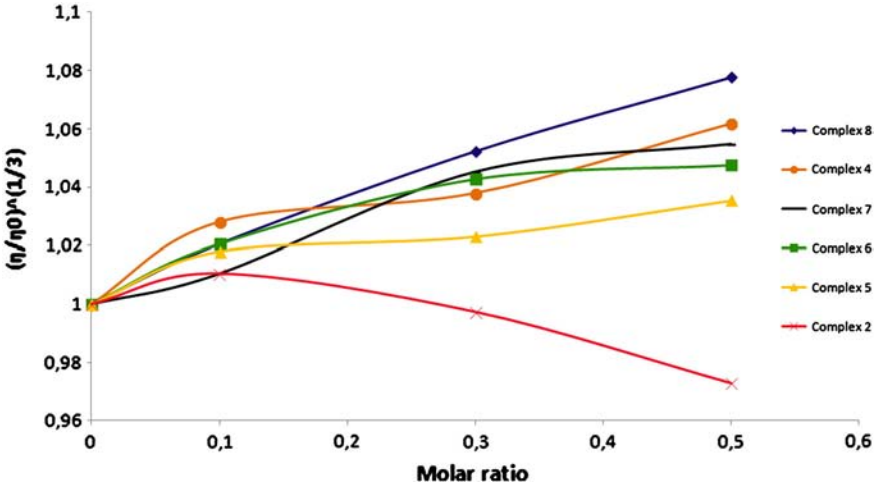

Fig. 10. Viscosity evolution for calf thymus DNA solutions treated with synthesized ruthenium complexes.

instrumental conditions. Significant changes in CCS should be evaluated as they reflect conformational changes that could affect some functions of the protein. More detailed information about IMS–MS can be found in the literature [48].

As mentioned before, PCI protein can act as a vehicle for anticancer drugs towards specific cancer cells in case the binding of the metal complexes doesn't distort the protein structure, since it is an antagonist of EGFs. With the aim of studying the conformational changes of PCI and ubiquitin due to the ruthenium complexes binding IMS–MS experiments were carried out.

MS spectra shown in Fig. 14 demonstrate the binding of different fragments of ruthenium complexes to both PCI and ubiquitin, and reinforce previous conclusions out of HPLC–MS studies. As can be seen, again, the presence of PPh_3 moiety affords slower kinetics and smaller yields of protein–metal complex binding, which should have important consequences in terms of drug distribution and detoxification mechanisms.

Table 2 shows the CCSs obtained when relating the drift times out of the IMS–MS experiments for each molecule reaching the detector, with the cross section calibration curve made with protein standards (see also Fig. S2 in the Supplementary information).

As shown in the table, the differences in CCS upon ligand interaction with UBI and PCI lay between 0.02 and 11.7% which suggests no significant conformational changes in the three-dimensional gas-phase protein

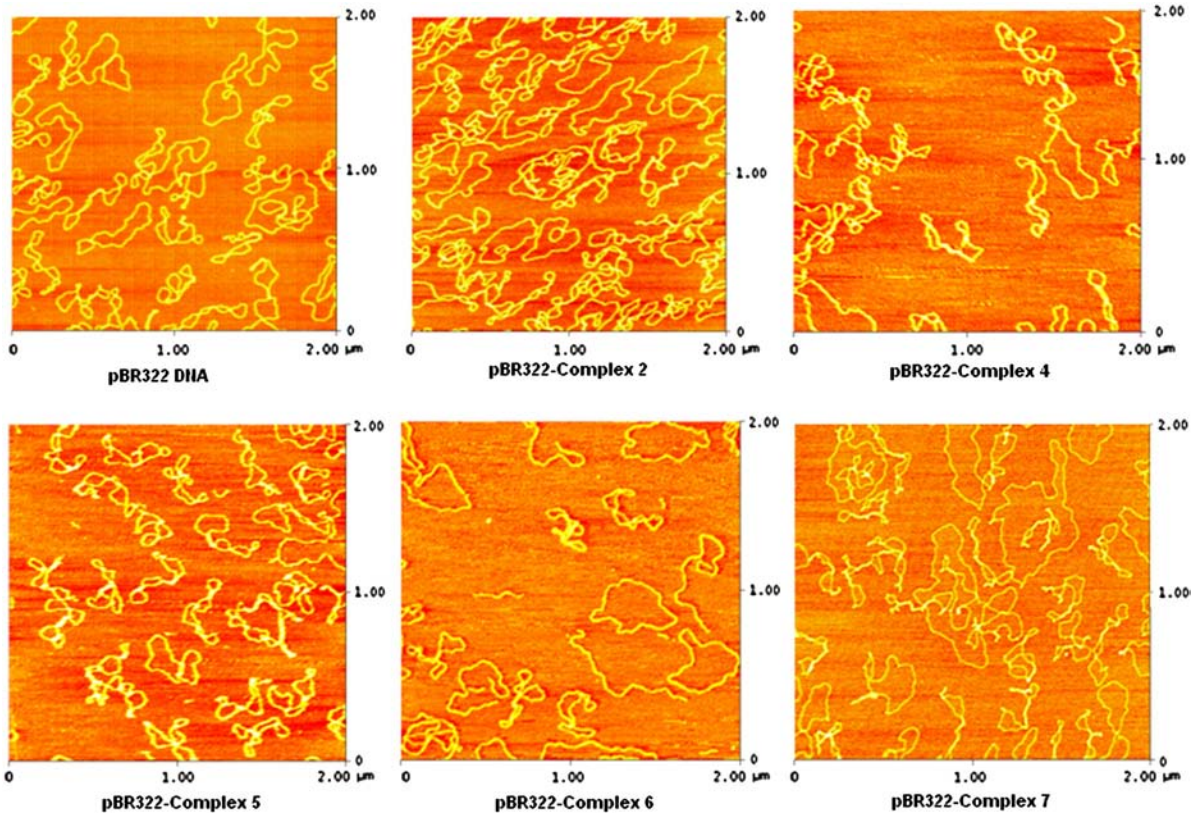

Fig. 11. Atomic force microscopy (AFM) images of pBR322-DNA plasmid solutions treated with synthesized ruthenium complexes.

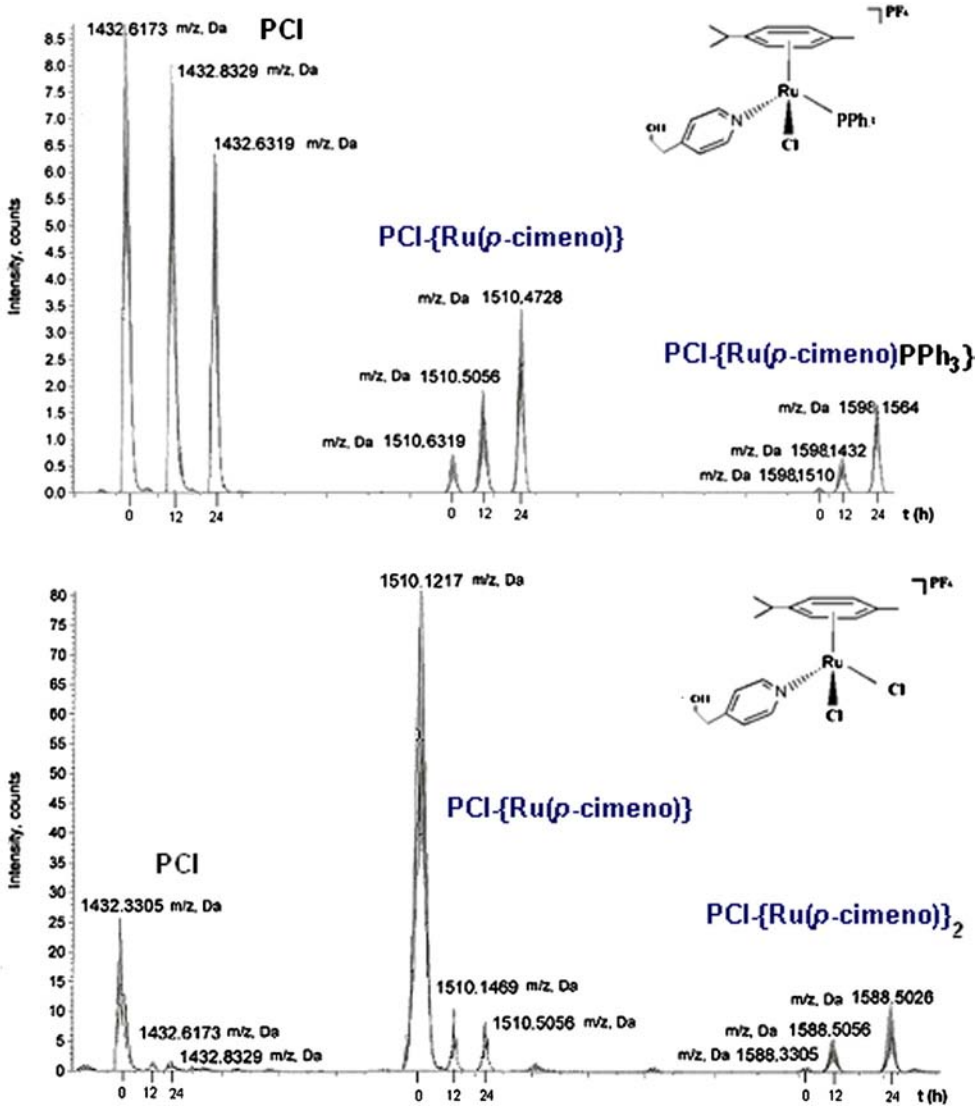

Fig. 12. HPLC–MS tuned spectra of PCI-complex **2**, **7** solution. Go to Supplementary information Fig. S6 to see all complete mass spectra.

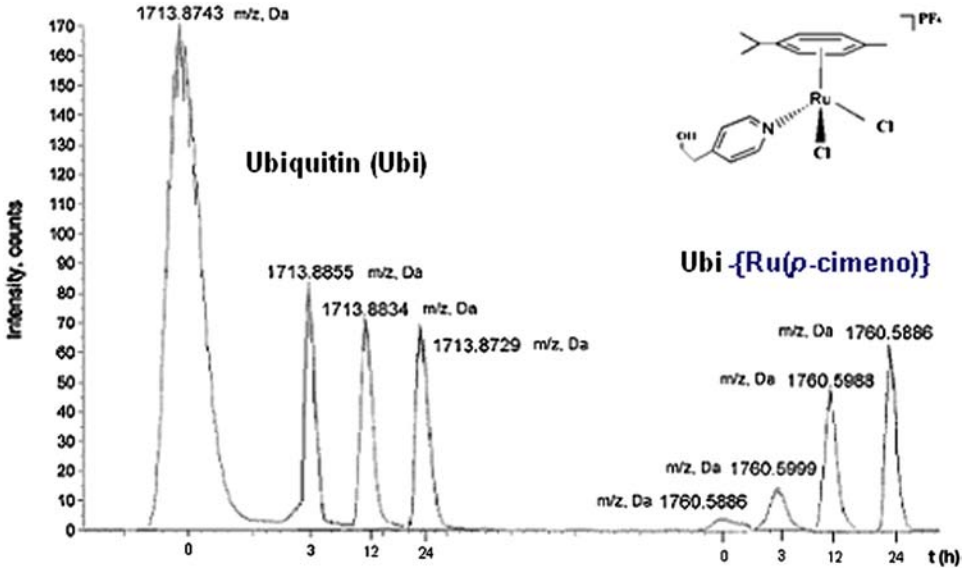

Fig. 13. HPLC–MS tuned spectra of Ubi-complex **2** solution. Go to Supplementary information Fig. S6 to see all complete mass spectra.

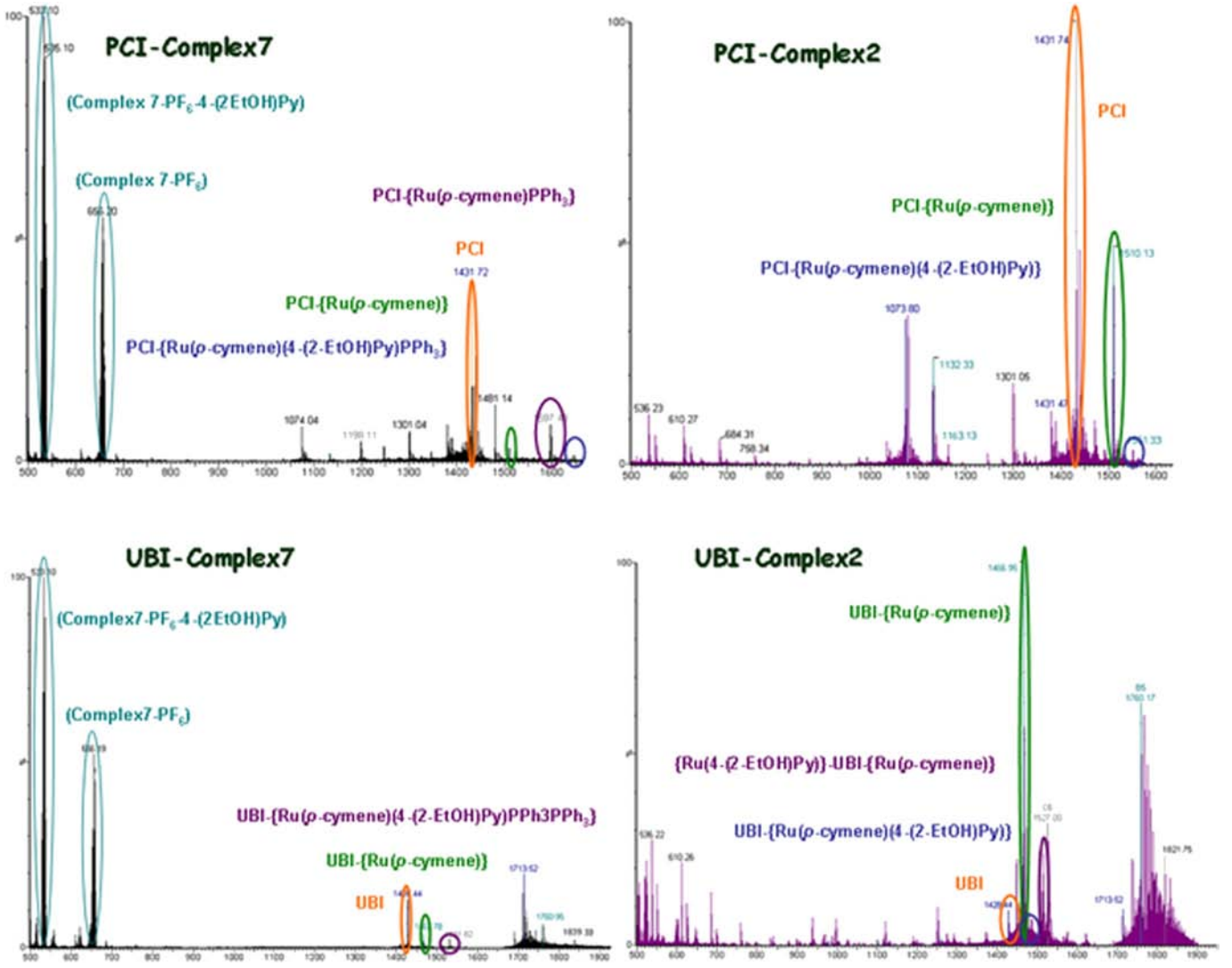

Fig. 14. MS spectra of PCI, UBI, complex **2** and complex **7** combination solutions.

structure. That would support both the possibility of drug delivery by model proteins as ubiquitin and the possibility of specific vehiculization towards cancer cells by specific proteins as PCI.

3.3. Cytotoxicity studies

Cytotoxicity studies were carried out for complexes **2**–**7** in HL_{60} Human Leukemia Tumor Cell Line, affording IC_{50} values shown in Table 3.

Table 2
Cross-section variations of different detected adducts. (a) No DMSO in solution. (b) 2% DMSO in solution.

Molecule	Adduct	CCS (Å^2)	ΔCCS %
PCI (a)	–	545	–
PCI (b)	–	569	–
PCI (b)-2	PCI (b)-[Ru(*p*-cymene)]	584	2.5
PCI (b)-2	PCI (b)-[Ru(*p*-cymene)PPh3]	596	4.5
PCI (a)-7	PCI (a)-[Ru(*p*-cymene)]	566	3.7
UBI (a)	–	1015	
UBI (b)	–	1017	
UBI (b)-2	UBI (b)-[Ru(*p*-cymene)]	1028	1.1
UBI (b)-2	UBI (b)-[Ru(*p*-cymene)PPh3]	1015	0.02
UBI (a)-7	UBI (b)-[Ru(*p*-cymene)]	908	11.7

The cytotoxic properties of the complexes including PPh_3 ligand in its structure correspond to values comparable to the cytotoxicity obtained for *cis*-platin and ruthenium complexes active against cancer cell lines in similar experiments [49] (notice that ruthenium complexes undergo some special processes, such as hydrolysis and different bindings compared to *cis*-platin), while the only one that lack this moiety raises over 200 μM, so it cannot be considered an active drug towards this type of tumor cell line.

These results added to the fact that previous investigations carried out in our group [50] in which most of the complexes studied in the present work, but lacking PPh_3 moiety, were evaluated as antitumor drugs showing poor antiproliferative properties, strongly suggest an important increment of the antitumor properties of ruthenium complexes due to PPh_3 presence.

Table 3
IC50 values at 24 h for HL60 leukemia tumor cell line.

Complex	IC_{50} (μM)
Complex **2**	202
Complex **4**	10.1
Complex **5**	5.2
Complex **6**	5.2
Complex **7**	15.4

4. Conclusions

Several new organometallic ruthenium complexes, some of them including PPh_3 ligands, have been synthesized and characterized. DNA interaction studies have demonstrated the capability of these complexes to bind DNA and distort its secondary and tertiary structure notably. Ethidium bromide displacement experiments and viscosity measurements prove that those complexes including PPh_3 moiety in its structure are able to intercalate into DNA base pairs, whereas those without PPh_3 ligand bind DNA only in a covalent manner. Protein interaction studies have shown the capability of these complexes to bind as well as to model and specific proteins, demonstrating slower kinetics and smaller binding yields when PPh_3 group is present, presumably due to steric impediments. These effects could have important consequences in drug cell up-taken and/or detoxification mechanisms. Finally, cytotoxicity studies show that IC_{50} values in the range of the ones obtained for *cis*-platin, considered a positive control for antiproliferative tumor cell studies, in all cases except for the complex lacking PPh_3 ligand. That result proves definitively the increment of ruthenium complex antiproliferative potential due to the PPh_3 presence, presumably owing to its capability to intercalate between DNA base pairs. Therefore IMMS studies demonstrate no change in conformational structure of the proteins due to ruthenium complex binding which supports a possible role of PCI as a vehiculizing agent to specific tumor cells for ruthenium complexes.

Acknowledgments

Financial support from the Spanish Ministry of "Ciencia e Innovación", contracts CTQ2008-02064 and BIO2010-22321-C02-01 is kindly acknowledged.

Appendix A. Supplementary data

Supplementary data to this article can be found online at http://dx.doi.org/10.1016/j.jinorgbio.2014.03.002.

References

[1] G. Süss-Fink, Dalton Trans. 39 (2010) 1673–1688.
[2] V. Brabec, O. Nováková, Drug Resist. Update 9 (2006) 111–122.
[3] W.J. Zeller, S. Fruhauf, G. Cheng, B.K. Keppler, E. Frei, M. Kaufmann, Eur. J. Cancer 27 (1991) 62–67.
[4] M. Coluccia, G. Sava, F. Loseto, A. Nassi, A. Boccarelli, D. Giordano, E. Alessio, G. Mestroni, Eur. J. Cancer 29A (1993) 1873–1879.
[5] M.J. Clarke, Coord. Chem. Rev. 236 (2003) 209–233.
[6] E. Alessio, G. Mestroni, A. Bergamo, G. Sava, Curr. Top. Med. Chem. 4 (2004) 1525–1535.
[7] Y.K. Yan, M. Melchart, A. Habtemariam, P.J. Sadler, Chem. Commun. (2005) 4764–4776.
[8] A.D. Phillips, O. Zava, R. Scopelitti, A.A. Nazarov, P.J. Dyson, Organometallics 29 (2010) 417–427.
[9] P.C.A. Bruijnincx, P.J. Sadler, Adv. Inorg. Chem. 61 (2009) 1–62.
[10] A.F.A. Peacock, P.J. Sadler, Chem. Asian. J. 3 (2008) 1890–1899.
[11] S.J. Dougan, P.J. Sadler, Chimia 61 (2007) 704–715.
[12] L. Ronconi, P.J. Sadler, Coord. Chem. Rev. 251 (2007) 1633.
[13] E. Aird, J. Cummings, A.A. Ritchie, M. Muir, R.E. Morris, H. Chen, P.J. Sadler, D.I. Jodrell, Br. J. Cancer 86 (2002) 1652.
[14] R.E. Morris, R.E. Aird, P.D. Murdoch, H.M. Chen, J. Cummings, N.D. Hughes, S. Parsons, A. Parkin, G. Boyd, D.I. Jodrell, P.J. Sadler, J. Med. Chem. 44 (2001) 3616.
[15] R. Fernandez, M. Melchart, E. Vand Der Geer, F. Wang, A. Habtemariam, P.J. Sadler, J. Inorg. Biochem. 96 (2003) 130.
[16] F. Wang, H. Chen, J.A. Parkinson, P.D. Murdoch, P.J. Sadler, Inorg. Chem. 41 (2002) 4509.
[17] R. Fernandez, M. Melchart, A. Habtemariam, S. Parsons, P.J. Sadler, Chem. Eur. J. 10 (2004) 5173.
[18] M. Melchart, A. Habtemariam, S. Parsons, P.J. Sadler, J. Inorg. Biochem. 101 (2007) 1903.
[19] G. Sava, S. Pacor, M. Coluccia, M. Mariggio, M. Cocchietto, E. Alessio, G. Mestroni, Drug Invest. 8 (1994) 150.
[20] O. Novakova, J. Kasparkova, O. Vrana, P.M. van Vliet, J. Reedijk, V. Brabec, Biochemistry 34 (1995) 12369.
[21] M.J. Clarke, F. Zhu, D.R. Frasca, Chem. Rev. 99 (1999) 2511.
[22] W.H. Hang, P.J. Dyson, Eur. J. Inorg. Chem. (2006) 4003–4018.
[23] I. Khailaila, A. Bergamo, F. Bussy, G. Sava, P.J. Dyson, Int. J. Oncol. 29 (2006) 261–268.
[24] C.S. Allardyce, P.J. Dyson, F.R. Abou-Shakra, H. Birtwistle, J. Coffey, Chem. Commun. (2001) 2708–2709.
[25] C.N. Pace, F. Vajdos, L. Fee, G. Grimsley, T. Gray, Protein Sci. 4 (1995) 2411–2423.
[26] T. Mosmann, J. Immunol. Methods 65 (1983) 55–63.
[27] N. Butenko, A.I. Tomaz, O. Nouri, E. Escribano, V. Moreno, S. Gama, V. Ribeiro, J.P. Telo, J.C. Pesssoa, I. Cavaco, J. Inorg. Biochem. 103 (2009) 622–632.
[28] G. Zhang, J. Guo, J. Pan, X. Chen, J. Wang, J. Mol. Struct. 923 (2009) 114–119.
[29] J. Sun, S. Wu, Y. An, J. Liu, F. Gao, L.-N. Ji, Z.-W. Mao, Polyhedron 27 (2008) 2845–2850.
[30] J.G. Liu, B.H. Ye, H. Li, Q.X. Zhen, L.N. Ji, Y.H. Fu, J. Inorg. Biochem. 76 (1999) 265.
[31] V. Brabec, Prog. Nucleic Acid Res. Mol. Biol. 71 (2002) 1–68.
[32] B. Lippert, Cisplatin: Chemistry and Biochemistry of a Leading Anticancer Drug, Wi1ey, New York, 1999.
[33] G. Pintus, B. Tadolini, A.M. Possadino, B. Sanna, M. Debidda, F. Bennardini, G. Sava, C. Ventura, Eur. J. Biochem. 269 (2002) 5861–5870.
[34] A. Bergamo, A. Masi, P.J. Dyson, G. Sava, Int. J. Oncol. 33 (2008) 1281–1289.
[35] S. Chatterjee, S. Kundu, A. Bhattacharyya, C.G. Hartinger, P.J. Dyson, J. Biol. Inorg. Chem. 13 (2008) 1149–1155.
[36] C. Gaiddon, P. Jeannequin, P. Bischoff, M. Pfeffer, C. Sirlin, J.P. Loeffler, J. Pharmacol. Exp. Ther. 315 (2005) 1403–1411.
[37] C. Blanco-Aparicio, M.A. Molina, S. Fernández-Salas, M.L. Frazier, J.M. Mas, E. Querol, F.X. Avilés, R. de Llorens, J. Biol. Chem. 273 (1998) 12370–12377.
[38] J.M. Mas, P. Aloy, M. Martí-Renom, B. Oliva, C. Blanco-Aparicio, M.A. Molina, R. de Llorens, E. Querol, F.X. Avilés, J. Mol. Biol. 284 (1998) 541–548.
[39] A. Martínez, V. Moreno, L. Sanglas, R. de Llorens, F.X. Avilés, J. Lorenzo, Bioorg. Med. Chem. 16 (2008) 6832–6840.
[40] A. Casini, G. Mastrobuoni, C. Temperini, C. Gabbiani, S. Francese, G. Moneti, C.T. Supuran, A. Scozzafava, L. Mesori, Chem. Commun. (2006) 156–158.
[41] C.G. Hartinger, A. Casini, C. Duhot, Y.O. Tsybin, L. Mesori, P.J. Dyson, J. Inorg. Biochem. 102 (2008) 2136–2141.
[42] A. Casini, C. Gabbiani, E. Michelucci, G. Pieraccini, G. Moneti, P.J. Dyson, L. Mesori, J. Biol. Inorg. Chem. 14 (2009) 761–770.
[43] R. Breitling, A.R. Pitt, M.P. Barret, Trends Biotechnol. 24 (2006) 543–548.
[44] G. Madalinski, E. Godat, S. Alves, D. Lesage, E. Genin, P. Levi, J. Labarre, J.C. Tabet, E. Ezan, C. Junot, Anal. Chem. 80 (2008) 3291–3303.
[45] J.C. Erve, W. Demaio, R.E. Talaat, Rapid Commun. Mass Spectrom. 22 (19) (2008) 3015–3026.
[46] J.P. Williams, J.A. Lough, I. Campuzano, K. Richardson, P.J. Sadler, Rapid Commun. Mass Spectrom. 23 (2009) 3563–3569.
[47] J.P. Williams, T. Bugarcica, A. Habtemariam, K. Giles, I. Campuzano, M. Rodger, P.J. Sadler, J. Am. Soc. Mass Spectrom. 20 (2009) 1119.
[48] B.T. Ruotolo, J.L.P. Benesch, A.M. Sandercock, S.J. Hyung, C.V. Robinson, Nat. Protoc. 3 (7) (2008) 1139.
[49] V. Moreno, J. Lorenzo, F.X. Aviles, M.H. Garcia, J.P. Ribeiro, T.S. Morais, P. Florindo, M. P. Robalo, Bioinorg. Chem. Appl. (2010) 936834.
[50] J. Grau, V. Noe, C. Ciudad, M.J. Prieto, M. Font-Bardía, T. Calvet, V. Moreno, J. Inorg. Biochem. 109 (2012) 72–81.